Silica Nanoparticle Crystals and Ordered Coatings Using Lys-Sil and a Novel Coating Device

Mark A. Snyder, J. Alex Lee, Tracy M. Davis, L. E. Scriven, and Michael Tsapatsis*

Department of Chemical Engineering and Materials Science, University of Minnesota, Minneapolis, Minnesota 55455

Received April 12, 2007. In Final Form: June 13, 2007

Silica nanoparticles with a narrow particle size distribution and controlled diameters of 10−20 nm are synthesized via hydrolysis and hydrothermal aging of tetraethylorthosilicate in an aqueous L-lysine solution. Cryo-transmission electron microscopy (cryo-TEM) reveals that the silica nanoparticles assemble to form close-packed nanoparticle crystals over short length scales on carbon-coated grids. Evaporative drying of the same sols results in nanoparticle stability and remarkable long-range facile ordering of the silica nanoparticles over scales greater than 10 μm. Whereas small-angle X-ray scattering (SAXS) and small-angle neutron scattering (SANS) discount the possibility of a core (silica)−shell (lysine) structure, the possibility remains for lysine occlusion within the silica nanoparticles and concomitant hydrogen bonding effects driving self-assembly. Facile ordering of the silica nanoparticles into multilayer and monolayer coatings over square-centimeter areas by evaporation-induced self-assembly is demonstrated using a novel dip-coating device.

I. Introduction

Silica nanoparticles are desirable for applications including membranes,[1−4] colloidal lithography,[5] core−shell nanoparticles for cancer therapy and diagnosis[6−10] and photonic applications,[11] drug and/or DNA delivery systems,[12−14] dye-doped nanoparticles for ultrasensitive bioanalysis,[15−19] tuned nanoparticle films as antireflective and antifogging coatings,[20−24] and building blocks of colloidal and nanoparticle crystals.[25] Such nanoparticles can be made by the Stöber process[26−28] in reverse micelles[29] and by other methods. However, controlling the size and monodispersity of silica nanoparticles in the 10 nm range through simple synthesis techniques has proven elusive until recently despite the prospect that such particles hold for surmounting limitations of scale associated with particle-based and thin-film technologies. A well-recognized alternative to the conventional techniques mentioned above is the formation of silica nanoparticles via hydrolysis of tetraethylorthosilicate (TEOS) in highly basic solutions in the presence of organic or inorganic cations.[30−35]

Recently, tetraethylorthosilicate (TEOS) hydrolysis in aqueous lysine solutions was introduced by Yokoi and co-workers[25] and our group[36] as a simple and more benign (i.e., lower pH) method of forming aqueous suspensions of monodisperse silica nanoparticles. We have previously reported[36] how the initial formation of these nanoparticles (i.e., rapid formation upon exceeding the silica solubility limit) parallels that observed for silica in the presence of strong bases.[31] In the case of the silica nanoparticles synthesized in lysine solutions, numerous handles exist (e.g., sol pH, temperature, silica content) for tuning particle size within the 5−20 nm range depending on composition and hydrolysis conditions. We named these sols Lys-Sil because they may consist, in their purest form, mainly of lysine, silica nanoparticles, and water.

Specifically, Davis et al.[36] reported room-temperature hydrolysis yielding particles with diameters in the 5−10 nm range

* Corresponding author. E-mail: tsapatsi@cems.umn.edu. Fax: 612-626-7246.

(1) Cichelli, J.; Zharov, I. *J. Am. Chem. Soc.* **2006**, *128*, 8130.
(2) Schepelina, O.; Zharov, I. *Langmuir* **2006**, *22*, 10523.
(3) Newton, M. R.; Bohaty, A. K.; Zhang, Y.; White, H. S.; Zharov, I. *Langmuir* **2006**, *22*, 4429.
(4) Bohaty, A. K.; Zharov, I. *Langmuir* **2006**, *22*, 5533.
(5) Yang, S.-M.; Jang, S. G.; Choi, D.-G.; Kim, S.; Yu, H. K. *Small* **2006**, *2*, 458.
(6) Brongersma, M. L. *Nat. Mater* **2003**, *2*, 296.
(7) Loo, C.; Hirsch, L.; Lee, M.-H.; Chang, E.; West, J.; Halas, N.; Drezek, R. *Opt. Lett.* **2005**, *30*, 1012.
(8) Loo, C.; Lin, A.; Hirsch, L.; Lee, M.-H.; Barton, J.; Halas, N.; West, J.; Drezek, R. *Technol. Cancer Res. Treat.* **2004**, *3*, 33.
(9) Loo, C.; Lowery, A.; Halas, N.; West, J.; Drezek, R. *Nano Lett.* **2005**, *5*, 709.
(10) O'Neal, D. P.; Hirsch, L. R.; Halas, N. J.; Payne, J. D.; West, J. L. *Cancer Lett.* **2004**, *209*, 171.
(11) Graf, C.; van Blaaderen, A. *Langmuir* **2002**, *18*, 524.
(12) Gemeinhart, R. A.; Luo, D.; Saltzman, W. M. *Biotechnol. Prog.* **2005**, *21*, 532.
(13) Roy, I.; Ohulchanskyy, T. Y.; Bharali, D. J.; Pudavar, H. E.; Mistretta, R. A.; Kaur, N.; Prasad, P. N. *Proc. Natl. Acad. Sci. U.S.A.* **2005**, *102*, 279.
(14) Roy, I.; Ohulchanskyy, T. Y.; Pudavar, H. E.; Bergey, E. J.; Oseroff, A. R.; Morgan, J.; Dougherty, T. J.; Prasad, P. N. *J. Am. Chem. Soc.* **2003**, *125*, 7860.
(15) Bertazza, L.; Celotti, L.; Fabbrini, G.; Loi, M. A.; Maggini, M.; Mancin, F.; Marcuz, S.; Menna, E.; Muccini, M.; Tonellato, U. *Tetrahedron* **2006**, *62*, 10434.
(16) Nyffenegger, R.; Quellet, C.; Ricka, J. *J. Colloid Interface Sci.* **1993**, *159*, 150.
(17) Ow, H.; Larson, D. R.; MSrivastava, M.; Baird, B. A.; Webb, W. W.; Wiesner, U. *Nano Lett.* **2005**, *5*, 113.
(18) Santra, S.; Zhang, P.; Wang, K.; Tapec, R.; Tan, W. *Anal. Chem.* **2001**, *73*, 4988.
(19) Zhao, X.; Bagwe, R. P.; Tan, W. *Adv. Mater* **2004**, *16*, 173.
(20) Cebeci, F. C.; Wu, Z.; Zhai, L.; Cohen, R. E.; Rubner, M. F. *Langmuir* **2006**, *22*, 2856.
(21) Hayes, R. A.; Bohmer, M. R.; Fokkink, L. G. J. *Langmuir* **1999**, *15*, 2865.
(22) Lee, D.; Rubner, M. F.; Cohen, R. E. *Nano Lett.* **2006**, *6*, 2305.
(23) Prevo, B. G.; Hwang, Y.; Velev, O. D. *Chem. Mater* **2005**, *17*, 3642.
(24) Yancey, S. E.; Zhong, W.; Heflin, J. R.; Ritter, A. L. *J. Appl. Phys.* **2006**, *99*, 034313.
(25) Yokoi, T.; Sakamoto, Y.; Terasaki, O.; Kubota, Y.; Okubo, T.; Tatsumi, T. *J. Am. Chem. Soc.* **2006**, *128*, 13664.
(26) Stober, W.; Fink, A. *J. Colloid Interface Sci.* **1968**, *26*, 62.
(27) Katelson, H. A.; Pelton, R.; Brook, M. A. *Langmuir* **1996**, *12*, 1134.
(28) van Blaaderen, A.; van Geest, J.; Vrij, A. *J. Colloid Interface Sci.* **1992**, *154*, 481.
(29) Osseo-Asare, K.; Arriagada, F. J. *Colloids Surf.* **1990**, *50*, 321.
(30) Cheng, C. H.; Shantz, D. F. *J. Phys. Chem. B* **2005**, *109*, 7266.
(31) Fedeyko, J. M.; Rimer, J. D.; Lobo, R. F.; Vlachos, D. G. *J. Phys. Chem. B* **2004**, *108*, 12271.
(32) Fedeyko, J. M.; Vlachos, D. G.; Lobo, R. F. *Langmuir* **2005**, *21*, 5197.
(33) Rimer, J. D.; Lobo, R. F.; Vlachos, D. G. *Langmuir* **2005**, *21*, 8960.
(34) Schoeman, B. J.; Regev, O. *Zeolites* **1996**, *17*, 447.
(35) Yang, S. Y.; Navrotsky, A.; Wesolowski, D. J.; Pople, J. A. *Chem. Mater.* **2004**, *16*, 210.
(36) Davis, T. M.; Snyder, M. A.; Krohn, J. E.; Tsapatsis, M. *Chem. Mater.* **2006**, *18*, 5814.

10.1021/la701063v CCC: $37.00
Published on Web 07/11/2007

that could be used to form gels, thin films, and xerogels with different porosity. Yokoi et al.[25] reported hydrolysis at higher temperature in the presence of octane, yielding nanoparticles with diameters in the 10−20 nm range that, upon high-temperature solvent evaporation and calcination, can form close-packed assemblies (i.e., nanoparticle crystals). We focus here on the facile formation of ordered nanoparticle crystals and mono- and multilayer coatings by room-temperature evaporation-induced self-assembly of Lys-Sil sols.

II. Experimental Section

Lys-Sil Nanoparticle Synthesis. Silica nanoparticles were synthesized via hydrolysis of tetraethylorthosilicate (TEOS, 98% Aldrich) in the presence of an aqueous solution of the amino acid L-lysine (Sigma-Aldrich), followed by hydrothermal aging. The molar composition of the Lys-Sil sols described herein was 60 SiO_2/x lysine/9500 water/240 ethanol, where the lysine content was varied between $x = 1.7$ and 5.8. These molar lysine limits correspond specifically to 25 and 85% of the lysine solubility in water. For clarity, representative examples reported here are drawn from the corresponding sols of these limiting cases. Specifically, the Lys-Sil sols were synthesized by the addition of the prescribed amount of TEOS to an aqueous lysine solution at 60 °C. Hydrolysis was carried out at 60 °C under vigorous stirring for 20 h. The hydrolyzed sol was then transferred to Teflon-lined stainless steel autoclaves and aged hydrothermally at 100 °C for 20 h to obtain Lys-Sil sols with an estimated nanoparticle volume fraction of approximately 1%.

In Situ Lys-Sil Sol Characterization. Small-angle X-ray scattering (SAXS) patterns were collected at room temperature (25 °C) with a SAXSess instrument (Anton Paar GmbH) employing Cu K_α radiation. Small-angle neutron scattering (SANS) analysis was also carried out at room temperature on the NG3 beam line located at the National Institute of Standards and Technology (NIST, Gaithersburg, MD). Scattering for each sample was measured at three source-to-detector distances (i.e., 13, 4, and 1 m) to span a q range of 4×10^{-3} to 0.5 Å^{-1}. For the purpose of increasing the contrast of lysine in the samples analyzed by SANS, partial molar substitution of deuterium oxide (D_2O, Cambridge Isotopes) for water was used. Cryo-transmission electron microscopy (cryo-TEM) was employed for direct imaging of Lys-Sil sols. Specimens were prepared following Talmon,[37] and images were collected using a JEOL 1210 TEM with a Gatan 613. The DH cooling holder operated at 120 kV.

Ex Situ Characterization of Dried Sols and Films. Scanning electron microscopy (SEM) was carried out on Pt-coated (approximately 50 Å) dried sols and films using a JEOL 6500 SEM. Film morphology was assessed by profilometry scans in the dipping direction of the coatings using a Tencor P10 profilometer.

Nanoparticle Coatings. Coatings of silicon substrates with Lys-Sil nanoparticles were realized with a novel coating apparatus designed to withdraw from a static nanoparticle sol a substrate at a controlled rate and under a prescribed flow of dry nitrogen. The draw rate, nitrogen flow rate (i.e., solvent evaporation rate), and sol concentration were all controlled during film deposition. Details of the device are included in Supporting Information and will be described further in a forthcoming communication.

Calcination of films was carried out over a range of temperatures using a ramp rate of 1 °C min^{-1} and an 8 h hold time.

III. Results and Discussion

In our previous work[36] on room-temperature hydrolysis of Lys-Sil sols, we reported decreasing pH with increasing silica content for compositions well above the silica solubility limit. We rationalized this to result from the sequestration of free lysine from solution by association with the silica nanoparticles. While not shown explicitly here, we have observed the persistence of this trend in pH even in the case of hydrolysis at 60 °C and Lys-Sil sol hydrothermal aging at 100 °C. The location of lysine, a basic amino acid, is of particular interest because of its potential to affect particle stability and particle charge and to induce particle−particle hydrogen bonding that could promote self-assembly.

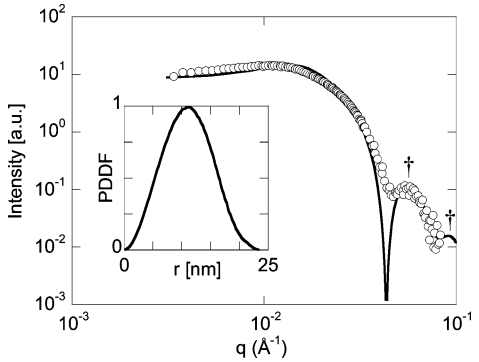

Figure 1. Comparison of desmeared small-angle X-ray scattering (SAXS) (solid curve) and small angle neutron scattering (SANS) (open symbols) results for a Lys-Sil sol of molar composition 60 SiO_2/5.8 lysine/2850 D_2O/6650 water/240 ethanol (1% by vol nanoparticles). The pair distance distribution function (PDDF) extracted from the desmeared SAXS data is shown in the inset.

We have employed SAXS and SANS measurements to probe the structure of the nanoparticles in terms of this possible lysine association. Here, we exploit the difference in contrast of lysine when probed by X-rays and neutrons, respectively, to investigate whether the Lys-Sil system mimics that of tetrapropylammonium (TPA)−silica, which is characterized by nanoparticles having a core (silica)−shell (TPA) structure.[31]

Figure 1 shows a comparison of typical SAXS and SANS data from Lys-Sil sols prepared by TEOS hydrolysis at 60 °C and followed by hydrothermal aging at 100 °C. The remarkable quantitative agreement between the SAXS and SANS data shown here, observed generally for all Lys-Sil sols characterized in this work, effectively rules out the possibility of a core−shell silica−lysine structure. It does not, however, discount other means of lysine association with the silica nanoparticles (e.g., direct incorporation of lysine in the silica core during hydrolysis). In fact, lysine association remains a plausible explanation for the observed decrease in pH with increasing silica content, and, by means of hydrogen bonding, for promoting the ordering (close packing) of the silica nanoparticles that we discuss later. Further exploration of the specific association of lysine with the silica nanoparticles is currently ongoing and will be reported elsewhere.

Nanoparticle size can be inferred from the desmeared SAXS (and SANS) data by extracting the corresponding pair distance distribution function (PDDF) through the method of indirect Fourier transformation.[38,39] The associated PDDF for the case considered, shown in the inset of Figure 1, suggests that the particles are on the order of approximately 20 nm in diameter. Data collected for sols of different silica and lysine compositions considered in this work (not shown) suggest that nanoparticles formed via hydrolysis at 60 °C and aging at 100 °C can be tuned to sizes as small as 10 nm in diameter, such as those that we explore later in this work for nanoparticle coatings. It is clear that hydrolysis at 60 °C followed by aging at 100 °C generally results in larger particles than the 5−10 nm ones formed during room-temperature hydrolysis.[36]

(37) Talmon, Y. *Modern Characterization Methods of Surfactant Systems*; Marcel Dekker: New York, 1999.

(38) Glatter, O. *J. Appl. Crystallogr.* **1977**, *10*, 415.

(39) Glatter, O. *J. Appl. Crystallogr.* **1979**, *12*, 166.

(40) Lee, J. A.; Meng, L. L.; Norris, D. J.; Scriven, L. E.; Tsapatsis, M. *Langmuir* **2006**, *22*, 5217.

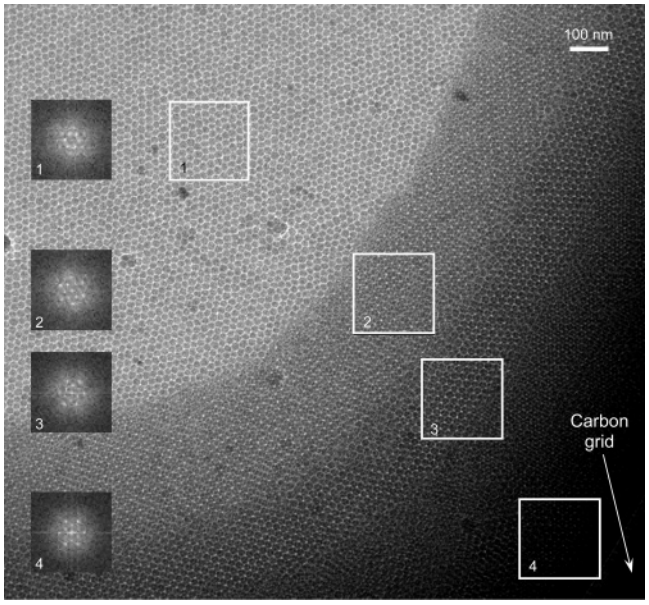

Figure 2. Cryo-TEM image of ordered nanoparticles in a vitrified Lys-Sil sol (60 SiO_2/5.8 lysine/2850 D_2O/6650 water/240 ethanol; 1% by vol nanoparticles) in the vicinity of a carbon grid. Progressively darker bands of nanoparticles observed in moving toward the carbon skeleton correspond to the development of close-packed multilayers with increasing sample thickness. Fourier transforms of regions (white boxes) within each band are shown as insets on the left.

A common distinguishing feature of the scattering curves for Lys-Sil samples made at elevated temperatures (as opposed to room-temperature hydrolyzed samples)[36] is the higher-order maxima present in both SAXS and SANS data, denoted by † symbols in the example shown in Figure 1. These maxima are a signature of the high degree of monodispersity of the nanoparticles, which may be important for the formation (close packing) of nanoparticle crystals that we describe below as well as for other applications.

Figure 2 shows a cryo-TEM image of the same sol discussed in Figure 1. The image depicts the remarkable ordering of the nanoparticles in a region close to the carbon skeleton of the grid used as a support in TEM imaging. We have observed the nanoparticle packing phenomenon generally in cryo-TEM images of samples that have undergone hydrolysis at 60 °C both with and without subsequent hydrothermal aging. This phenomenon, however, has not generally been observed for room-temperature hydrolyzed Lys-Sil sols of compositions consistent with those described previously.[36] Fourier transforms computed from several regions of the vitrified sol, shown as insets in Figure 2, are consistent with a close-packed, long-range-ordered arrangement.

The high particle densities and ordered arrangements observed in the vicinity of the carbon grid are in striking contrast to the conditions elsewhere in the vitrified sol (Figure S1, Supporting Information). Namely, in the case of hydrolysis at 60 °C, a decrease in packing density is generally observed far away from the carbon grid, where distinct silica nanoparticles suspended in the vitrified sol can be observed. In the case studied here, a stark contrast between the nanoparticle arrangement in regions close to and far from the carbon skeleton of the holey TEM grid may result, at least in part, from the technique used to prepare the cryo-TEM samples.[37] Namely, the impregnation of the grid with sol and subsequent blotting of the grid before vitrification naturally gives rise to regions (i.e., films) of varying thickness of the retained concentrated sol. Figure 2 clearly shows the progressive, stepped development of close-packed nanoparticle multilayers in the vicinity of carbon skeletons of the TEM grid. In these cases, the thickness and concentration of the Lys-Sil sol before vitrification appear to impart size selection to the progressive addition of monolayers.

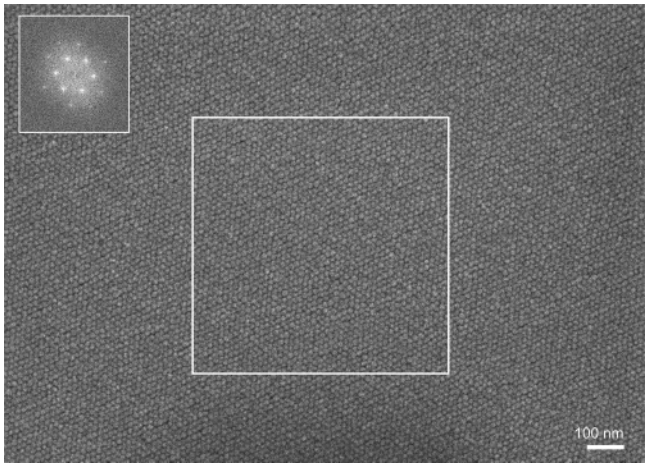

Figure 3. SEM image of a Lys-Sil sol (molar composition 60 SiO_2/5.8 lysine/2850 D_2O/6650 water/240 ethanol) after evaporative drying. The inset shows a Fourier transform pattern computed from the highlighted region (square outline).

An SEM image of the same sol after drying on carbon tape by room-temperature solvent evaporation is shown in Figure 3. The presence of distinguishable nanoparticles in the dried sol underscores the nanoparticle stability during drying. This stability may be a combined result of the buffering action of lysine during solvent evaporation and silica condensation promoted by hydrolysis at 60 °C and hydrothermal aging. We are interested here in the particle stability primarily because it enables the striking ordering, confirmed by Fourier transform of the highlighted region in Figure 3, of the dried nanoparticles into a nanoparticle crystal. As in the case of the cryo-TEM images, it indicates a close-packed arrangement of nanoparticles. Even more remarkable is the extent of the ordering, stretching well beyond what is even captured by the scale of the image in Figure 3 (Figure S2, Supporting Information); ordering in these dried sols is observed for regions spanning tens of micrometers.

Similar ordering of silica nanoparticles has been shown by Yokoi and co-workers[25] to occur in 1−3 μm crystals. In that work, however, sols consisted not only of silica and lysine but also of octane, and high-temperature solvent evaporation and calcination were required. The simplicity of the Lys-Sil sols (i.e., consisting primarily of lysine, silica, and water) stands to facilitate a clearer evaluation of mechanisms driving the facile assembly described herein. Although we have employed the as-made Lys-Sil sols throughout this work to realize the assembly of nanoparticle crystals and coatings, it is possible to purify the sols further through dialysis against water. This technique removes free lysine from solution and reduces the pH of the sols from an initial range of 9.5 to 10 to a final range of approximately 6 to 7 with no substantial change in the silica nanoparticles as probed by SAXS (not shown).

For the remainder of this letter, we look to exploit the facile ordering of dried silica nanoparticles for simple, large-scale, continuous coating of substrates. To realize such films, we employ a novel coating apparatus that is capable of simultaneously controlling the rates of coating and sol evaporation, which are two important parameters governing film thickness and coating continuity. A schematic describing the main operating principles of the coating device is shown in Figure 4c, with further details

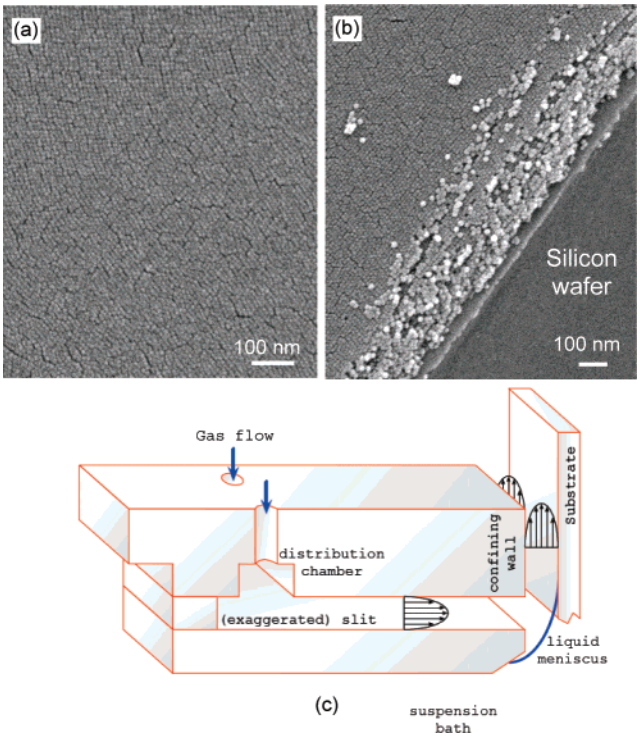

Figure 4. SEM images of the (a) surface and (b) cross section of a silica nanoparticle film resulting from coating a Lys-Sil sol of molar composition 60 SiO_2/1.7 lysine/9500 water/240 ethanol (1% by vol nanoparticles) on a silicon wafer using a novel coating device shown schematically in part c. Coating the silicon substrate was carried out at a rate of 20 cm h^{-1} under a flow of 3 SCFH of N_2 (distributed across the meniscus by a horizontal slit).

of the device given in Supporting Information and in a forthcoming communication.

Figure 4a,b shows top and cross-sectional SEM images, respectively, of a thick film composed of silica nanoparticles. The film was fabricated by room-temperature coating of a silicon support with the as-synthesized Lys-Sil sols reported herein. Coating was carried out at a rate of 20 cm h^{-1} and under a flow of 3 SCFH of nitrogen. The top view of the film (Figure 4a) shows close-packed domains of nanoparticles, reminiscent, albeit on a shorter length scale, of the result of static room-temperature evaporation (Figure 3). These domains of ordered nanoparticles appear to be separated by small, nanometer-sized grain boundaries with a slight orientation mismatch occurring between adjacent domains.

The presence of only short-range ordering under coating conditions, as opposed to the long-range ordering observed in the much thicker dried droplets (Figure 3) indicates that competition between dipping speed and the rate of particle rearrangement at the drying front may destroy long-range ordering. The cross-sectional image of the film, however, clearly shows that it consists of distinct layers of close-packed silica nanoparticles. The coating conditions in this case were such that a continuous, multilayered film on the order of 100 nm in thickness resulted. This film thickness appears to be well enough below critical dimensions that no apparent superficial changes (e.g., cracking and peeling) occurred upon subsequent calcination to temperatures as high as 700 °C.

The ultimate goal for such coatings from an applications standpoint is the reduction in film thickness toward an ordered nanoparticle monolayer film that is continuous over large regions, a task that has remained elusive. As discussed in ref 40, control of the nanoparticle concentration in the sol is one key parameter,

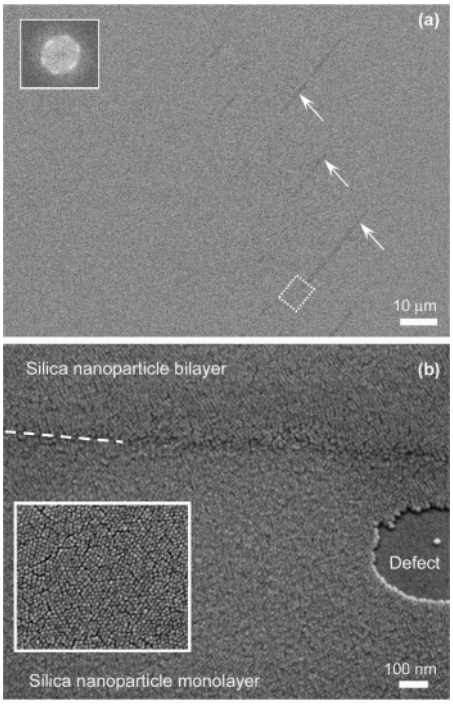

Figure 5. SEM images of a nanoparticle film resulting from coating Lys-Sil sols of molar composition 60 SiO_2/1.7 lysine/3.7 × 10^5 water/240 ethanol (0.02% by vol nanoparticles) on a silicon wafer. Dip coating was carried out at 6 cm h^{-1} under a flow of 3 SCFH of N_2. Panel a shows a nearly continuous film (defects denoted by arrows), and panel b shows a higher-magnification image corresponding to the outlined region in panel a. In panel b, the sample has been tilted during imaging to emphasize the bilayer-to-monolayer step (step edge marked partially by a dashed line). The inset in panel b shows a top view of the monolayer depicting the local ordering confirmed by the representative Fourier transform pattern shown as an inset in panel a.

in addition to dipping rates and the solvent evaporation rate (i.e., by adjusting nitrogen flow), affecting film thickness. Systematic studies in which coating conditions were varied have elucidated a parametric map of the combined role of these parameters in tuning the film thickness, coating continuity, and onset of discontinuous, quasi-periodic patterning. Details of this study are beyond the scope of this work and will be reported elsewhere.

Here, we focus on the successful realization of near-monolayer and semiordered coatings of silica nanoparticles over square-centimeter areas of substrate. Figure 5 shows SEM images of a representative nanoparticle film resulting from coating a silicon substrate at a rate of 6 cm h^{-1} under a flow of 3 SCFH of N_2 using a dilute form of the as-made sol (i.e., nanoparticle volume fraction of approximately 0.02%). Only infrequent defects in the films (i.e., exposing the bare silicon substrate, arrows in Figure 5a and labeled region in Figure 5b) are observed running perpendicular to the coating direction, with the large majority of the film characterized by a continuous monolayer or bilayer arrangement of silica nanoparticles. Representative profilometry traces along the direction of the coating are shown in Figure 6 and clearly depict the presence of a nearly continuous monolayer with bilayer outcroppings (Figure 6a) consistent with the SEM image of the same film in Figure 5b. Very infrequent development of trilayers (Figure 6b) can be observed, but in all cases, they disappear shortly after nucleation.

Domains of ordered silica nanoparticles are again present in these near-monolayer films (inset in Figure 5b). The smeared Fourier transform pattern computed from lower-magnification images of this coating (inset in Figure 5a) confirms the partial

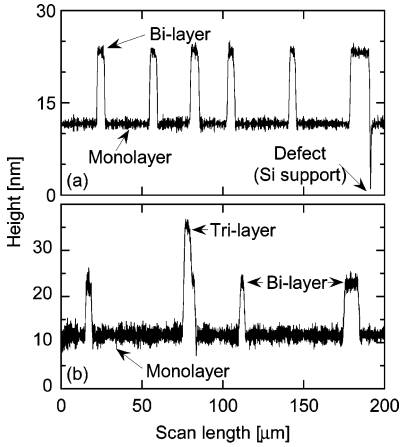

Figure 6. Profilometry scans along the dipping direction of nanoparticle films resulting from coating the Lys-Sil sol of molar composition 60 SiO_2/1.7 lysine/3.42 × 10^5 water/240 ethanol (0.02% by vol nanoparticles) on a silicon wafer at 6 cm h^{-1} and under a flow of 3 SCFH of N_2. Panel a shows a representative profilometry scan of the film with bilayer outcroppings and one defect exposing the silicon support. Panel b shows a scan revealing an infrequent trilayer in addition to the monolayer and bilayers.

ordering of these films. This local ordering may be a manifestation of lysine-induced hydrogen bonding between nanoparticles as well as particle monodispersity, both of which are believed to play a role in long-range ordering in the case of static evaporation. However, the extent of the ordering in the near-monolayer films is limited, possibly by the competition of these driving forces for assembly with capillary forces upon drying. Nonetheless, the ability to deposit, for the first time, a near-monolayer film of monodisperse silica nanoparticles with local ordering has exciting implications for thin films and other material applications. The formation of similar multilayer and monolayer particulate films using smaller Lys-Sil nanoparticles such as those discussed in ref 36 is currently under investigation.

In this work, we have employed Lys-Sil sols hydrolyzed at 60 °C and hydrothermally aged to achieve (1) highly monodisperse silica nanoparticles that are stable in the dried state, (2) facile nanoparticle ordering upon sol vitrification and evaporative drying, and (3) successful fabrication of multilayer and near-monolayer-ordered nanoparticle coatings over square-centimeter areas. The novelty of this work is derived from the elusiveness, until only recently,[25,36] of benignly synthesized monodisperse silica nanoparticles on the scales considered here and the consequential challenge of realizing silica nanoparticle crystals and large-area coatings. Enhancing the impact of the findings is the simplicity of the Lys-Sil synthesis and the existence of multiple handles (i.e., silica content, pH, hydrolysis, and aging temperature) for tailoring particle size. As such, we believe that these findings stand to impact, among others, the arenas of selective coatings and membranes (either nanoparticle- or replica-based), colloidal lithography, and chemical sensing and may even extend into the biological arena (e.g., leveraging facile in situ and ex situ ordering for cell encapsulation and anti-immunorejection coatings for implants) where applications and devices with tuned particle size, porosity, order, and monolayer continuity are critical.

Acknowledgment. Funding from the National Science Foundation (CTS-0522518) and IPrime is gratefully acknowledged. Characterization was carried out at the University of Minnesota Characterization Facility, which receives support from NSF through the National Nanotechnology Infrastructure Network.

Supporting Information Available: Details of the novel coating device shown schematically in Figure 4c and additional cryo-TEM and SEM images of silica nanoparticle crystals. This material is available free of charge via the Internet at http://pubs.acs.org.

LA701063V